Available online at www.sciencedirect.com

ScienceDirect

Procedia Structural Integrity 42 (2022) 480–489

Structural Integrity Procedia

www.elsevier.com/locate/procedia

23 European Conference on Fracture – ECF23

Investigation on the fatigue resistance of thick transverse attachments and design of VA fatigue tests

Davide Leonetti[a,*], Yukina Takai[b], Koji Kinoshita[b], Alain Nussbaumer[a]

[a] *Eindhoven University of Technology, Eindhoven, The Netherlands*
[b] *Gifu University, Gifu, Japan*
[c] *École Polytechnique Fédérale de Lausanne, Lausanne, Switzerland*

Abstract

The fatigue strength of structural steel components subjected to cyclic loading is often characterized in terms of S-N curves derived under constant amplitude (CA) loading. However, these are often subjected to load histories of variable amplitude and mean stress, i.e. variable amplitude (VA) loading. To take into account this loading condition for the design or the verification of structural components, damage accumulation models and modification of S-N curves have been proposed in the literature. However, these models require experimental characterization to verify or eventually calibrate some model parameters, e.g. the critical value of the Palmgren-Miner damage, among others.

This paper investigates the CA fatigue behavior of transverse welded steel attachments by reporting on an experimental characterization. Fatigue cracks have been monitored and fracture surfaces analyzed to obtain information about nucleation sites and growth rates. Moreover, the paper reports on the design of VA fatigue tests using a load history obtained from traffic measurements from a Swiss road bridge. As a design tool, the preliminary study using advanced probabilistic fatigue prediction models calibrated on similar welded details is presented. This model can also be used to define other load spectra to be applied in future VA experimental studies.

Keywords: Type your keywords here, separated by semicolons ;
Transverse attachments; Variable amplitude loading; Fatigue tests; Bridge structures

1. Introduction

The determination of the fatigue strength of structural connections, such as welded joints, inevitably requires experimental characterization due to the complex geometry, non-homogeneous material properties, and residual stresses, besides the potential presence of technological defects Gurney (1979); Lassen and Recho (2013). A large number of

* Corresponding author
E-mail address: d.leonetti@tue.nl

10.1016/j.prostr.2022.12.061

studies focus on the experimental characterization of fatigue resistance under constant amplitude loading, allowing the determination of stress-life curves, i.e. Wöhler curves or S-N curves, which are at the basis of current design codes for (welded) steel structures, such as EN 1993-1-9:2006 (2006); Hobbacher et al. (2016), among others. Another important aspect concerns the characterization of the fatigue resistance under operational loading, which is of variable mean stress and amplitude, i.e. variable amplitude loading. In fact, the majority of engineering structures are subjected to this type of loading, and more rarely to constant amplitude loading. Moreover, variable amplitude stress histories also differ depending on the specific application, and a prediction of the fatigue life under variable amplitude loading is not possible by just employing constant amplitude S-N curves and a cumulative damage hypothesis Sonsino (2007).

Variable amplitude load histories are often reduced to a stress spectrum by employing cycle counting techniques such as the Rainflow, Matsuishi and Endo (1968). A stress spectrum is often shown as cumulative frequency distribution, or an exceedence diagram, Haibach (1971); Gurney (2006). In both cases, the number of exceeding, either normalized or not, is related to the stress range, which can be also normalized. This results that each stress range is related to the times that this is exceeded. It has been extensively shown that different shapes of these spectra are related to different applications. For example, it has been shown that traffic loading on short-span bridges determines stress spectra following the shape of the Rayleigh distribution, Klippstein and Schilling (1976). From these observations, many variable amplitude fatigue tests were conducted in the US to characterize the fatigue resistance of welded joints, e.g. Fisher et al. (1983); Fisher (1993); Klippstein and Schilling (1989); Tilly and Nunn (1980). A comprehensive critical review of these tests is made in Albrecht and Lenwari (2009). In any of these test programs, an assumption was made to ensure the continuity of the load history reproduced during testing. In other words, randomly sampling stress ranges from a Rayleigh distribution does not ensure the continuity of the signal which has to be reproduced by the testing system. Therefore, load histories are often reproduced either with constant minimum stress or constant mean value. Another option is to perform typical constant amplitude block programs, e.g. as in Banno and Kinoshita (2022), a method that is also contemplated in the international standard ISO 12110-1:2013 (2013).

It is recognized that one of the disadvantages of the Rainflow counting method is that the order of the cycles disappears. This is of crucial importance for the reconstitution of the load histories, Sonsino (2004). With this perspective, the international standard ISO 12110-1:2013 (2013) also prescribes an alternative way to define the load history to be applied during a testing program. This involves the definition of a transition matrix reporting the number of transitions from level i to level j at the intersection of the line i and column j. This method has been used in previous investigations, see Gurney (2006). The random arrangement has an important influence on the experimental fatigue life, e.g. it is known that the block arrangement leads to a higher fatigue life, due to coaxing effects, Sonsino (2004).

The scope of this paper is two-fold. On the one hand, it reports an investigation of the fatigue performance of transverse attachments under constant amplitude loading, which serves as a preliminary step for a (future) variable amplitude test program. On the other hand, it shows the generation of a traffic load history to be applied in such a test program, including cleansing and simplification of the load history measured directly from the Venoge Bridge, a highway bridge, subjected to traffic loading.

2. Methods

This section describes the CA fatigue test data setup, the monitoring system installed on the Venoge Bridge, and the method developed to analyze and reduce the load history.

2.1. Experimental setup

This section provides a description of the specimen and the test setup in which the constant amplitude fatigue tests have been conducted.

2.1.1. Specimen

The transverse attachment specimen considered in this study is depicted in Figure 1a. It is made of S690QL structural steel and consists of a loading plate (main plate), and the stiffener plate (attachment plate), which is welded perpendicular to the loading plate in the center of it. The multi-pass 138 MAG-Flux cored metal-arc weld is executed using filler metal wire and gas according to ISO 18276. The cross-section of the main plate is reduced in the central

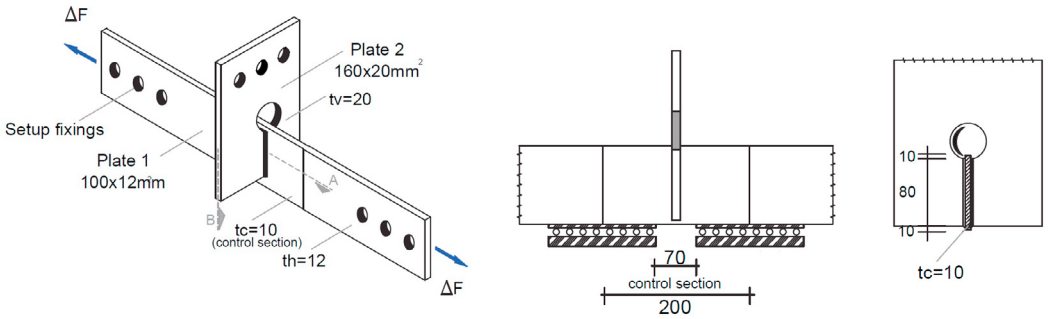

(a) Specimen (b) Section A (c) Section B

Fig. 1: Transverse attachment specimen used in the current investigation

part of the specimen, where the attachment plate is welded, determining the control section, see Figure 1b, to avoid premature failure of the specimen due to potential cracks growing at the bolt hole. Moreover, since the loading plate is 20mm wider than the portion of the attachment plate, see 1c, the weld is made all around the attachment plate. At each of the two ends, three holes allow the specimens to be clamped to the test frame, through three preloaded bolts, see also Figure 2a. This specimen has been used in previous studies conducted at EPFL, see Pereira Baptista (2016); Garcia (2020), where more information can be found about the monotonic and the cyclic material properties of the base metal, the heat affected zone, the weld metal and constant amplitude multiaxial fatigue tests. Moreover, it should be mentioned that attachments with thickness greater than the thickness of the main plate, although less investigated, are used in load introduction sections, or reinforced sections of bridge beams in correspondence with supports.

2.1.2. CA fatigue tests

The experiments have been carried out within an ad-hoc built testing frame anchored to the strong floor of the Structural Engineering Platform (GIS) at ENAC-EPFL. In particular, the load is applied by a hydraulic actuator with a capacity of 600kN, and the load is measured with a load cell of the same nominal capacity. The actuator is placed horizontally and is equipped with swivels both at the base and at the end of the rod. The specimen is connected using double-shear bolted connections with preloaded bolts to the end swivel. The alignment of the two connections, on the north and the south sides, has been checked through strain gauges mounted on both sides of the cover plates. The cyclic tests have been conducted by applying a time-varying sine load at a frequency of 3Hz, with a load ratio $R = 0.1$.

For each of the two weld toes located at the west locations, i.e. north-west and south-west, a stereoscopic digital image correlation (DIC) setup has been installed, see Figure 2b. An example of the speckle pattern realized on one of the monitored weld toes is given in Figure 2c. The cameras employed are manufactured from Manta, model G-235B PoE having a capacity of acquiring images at a maximum frequency rate of 50Hz, and are equipped with a 25 mm lens. The setup is such that a pixel corresponds to 5.86 μm. The camera trigger has been synchronized with the load signal, in order to capture the frame when the load is approximately at its maximum. The synchronization has been performed accounting for the delay in generating the trigger signal and the frequency streaming of the camera. This allows comparing images taken at approximately the same load level, and therefore with a fully open crack mouth. It should be mentioned that the post-processing of the DIC results is out of the scope of this paper.

2.2. Bridge monitoring data analysis

To obtain information concerning the traffic loading to be used in future VA fatigue test programs, the Venoge Bridge has been considered in this study. The Venoge Bridge is a composite road bridge located along Highway A1 (E25), between Lausanne and Geneva, in Switzerland. The original bridge has been built in 1966 and enlarged in 1997 allowing two more (heavy traffic) lanes per direction to be added. The strain history has been measured in two different locations on the main girder along the last span of the structure, in correspondence with the heavy traffic

(a) Clamped specimen (b) DIC setup, west locations (c) Speckle pattern

Fig. 2: Test setup

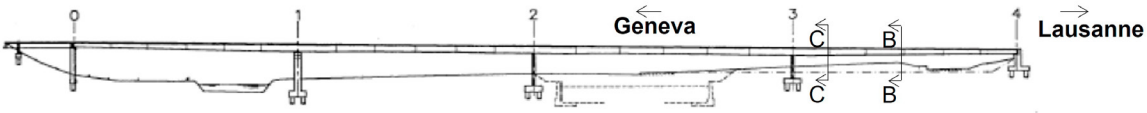

Fig. 3: Elevation of the Venoge Bridge, indicating the locations B and C along the main girder where the strain gauges are installed.

lane. Figure 3 depicts the elevation of the bridge, indicating the locations in which the strain gauges used in this study were installed.

Since the Venoge bridge is a statically indeterminate composite structure, internal stresses may arise in the case of uneven thermal expansion. In this study, the focus will be on the strains measured along the main girders supporting the bridge deck in the fourth span, in two locations: (a) close to the third pier, i.e. location C, and (b) in the center of the span, i.e. location B. Weldable strain gauges are employed, model HBWF-35-125-6-10-GP. Each weldable strain gauge is a full bridge configuration, with a resistance of 350 Ω. The full bridge configuration allows for the compensation of unconstrained thermal strains. Instead, the strains caused by uneven thermal elongation coefficients between the steel structure and the concrete deck, and non-uniform heating of the structure are measured.

The developed procedure to analyze and reduce the measured strain history consists of the following steps:

- Detrending
  This is necessary to filter the strain fluctuations due to the constrained thermal loads, which are not caused by the traffic. A piece-wise linear detrending is considered, in which the best-fitting line, in the least square sense, has been subtracted from the strain signal. In addition, the continuity of adjacent best-fitting lines has been guaranteed, thus ensuring that continuity is preserved for the detrended signal.
- Noise filtering
  A Butterworth low-pass filter with a cut-off frequency at 2Hz has been used for this purpose, resulting in the cancellation of the electric noise and small fluctuations. This cut-off frequency has been selected, by analyzing the content of the signal in the frequency domain, see Figure 4, where it can be observed that the most relevant amplitudes are up to 2 Hz.
- Range filtering
  The signal is transformed from the time domain into the sample domain by preserving solely peaks and troughs. A range filter size, see De Jonge (1982), is applied to filter low fluctuations. A peak at a certain level is only recognized as such if the signal has dropped to a level that is $\Delta\varepsilon_R$ lower than the peak level. In the same way, a trough is counted if the signal has risen $\Delta\varepsilon_R$ above the trough-level.
- Cycle counting
  The signal is statistically analyzed to derive the Markov transition matrix, which will allow the reconstitution of the strain-time history, i.e. re-sampling of the strain signal, see Sonsino (2004).

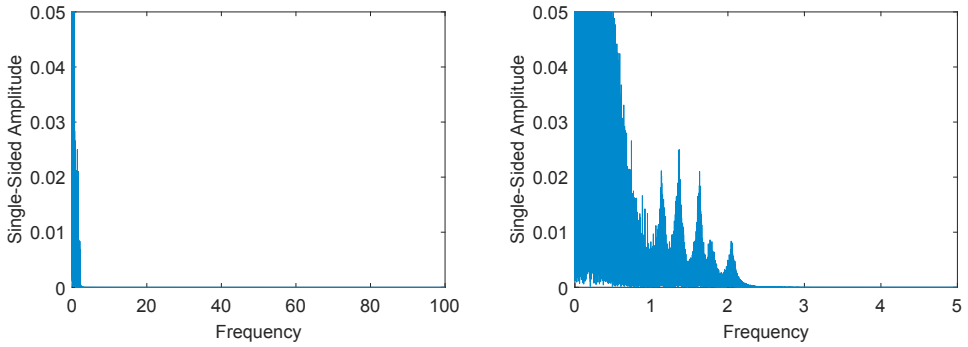

(a) Range 0-100Hz (b) Range 0-5Hz

Fig. 4: Example of the DFT for a strain signal, location B week 15.

As mentioned in Section 1, different authors indicated different strain or stress values to filter small strain ranges. In this work, since our goal is to produce test results with N comparable to the design life of bridges, this is defined as

$$\Delta\varepsilon_R = 0.25 \cdot \Delta\varepsilon_{0.25} \tag{1}$$

where $\Delta\varepsilon_{0.25}$ is the strain range corresponding 0.25% probability of being exceeded, and it is determined following a Rainflow counting of the strain signal after noise filtering. Other authors used $\Delta\varepsilon_{max}$ as a reference value to determine $\Delta\varepsilon_R$. In this paper, the former, i.e. Equation 1, is preferred for two reasons. The first reason is that this value is less scattered when calculated from strain signals with a one-week reference period. The second reason is associated with the observation made in Tilly and Nunn (1980) where the authors noted that a Rayleigh stress spectrum in which $\Delta\varepsilon_{0.25}$ corresponds to the fatigue limit, produced experimental lives in the order of the design fatigue life of steel bridges, i.e. $10^8 - 10^9$ cycles. Neglecting strain ranges lower than 25% of $\Delta\varepsilon_{0.25}$, when $\Delta\varepsilon_{0.25}$ corresponds to the fatigue limit of the detail under investigation $\Delta\varepsilon_D$, has a limited effect on the calculated fatigue damage. By considering an S-N curve as proposed in several standards, such as EN 1993-1-9:2006 (2006); Hobbacher et al. (2016), but without a cut-off limit, i.e. $\Delta\varepsilon_L = 0$, the damage accumulated by $\Delta\varepsilon \leq 0.25 \cdot \Delta\varepsilon_{0.25}$ is less than 1% of the critical damage. This is also in line with the results presented by Heuler who suggested filtering the strain ranges lower than 50% of the fatigue limit, see Heuler and Seeger (1986), as they observed that crack initiation life is longer when compared with the fatigue life under the unfiltered sequences. The same value of 50% of the fatigue limit is also used in Albrecht and Lenwari (2009) as a safe VA fatigue limit. It should be noted that such small strain fluctuations measured could be due to noise, and other types of loading such as vehicles riding on other lanes, wind, and light vehicles.

2.2.1. Markov transition matrix

The Markov transition matrix, also known as the probability matrix, is used to describe the transitions between troughs and peaks in a Markov process. Each element of the matrix $P_{i,j}$ indicates the probability of moving from position i to position j, i.e. $Pr(j|i)$. The two axes define the starting and finishing levels of each half-cycle and each individual element of the matrix indicates the number of half-cycles of each specific range. In this form of plot rising half ranges appear above the diagonal and falling half ranges below it. More details about it can be found in Gurney (2006); ISO 12110-1:2013 (2013); Sonsino (2004).

3. Results and Discussion

In this section, the results of the work are presented. First, the CA fatigue test data are reported including a preliminary analysis of the macroscopic fracture surface. Secondly, the analyses performed on the measured load history

Table 1: CA fatigue test results

Specimen ID	F_{min} [kN]	F_{max} [kN]	R [-]	$\Delta\sigma_{nom}$ [MPa]	N [cycles]	note
TA690-01	166.67	16.67	0.1	150	438113	DIC not installed
TA690-02	144.44	14.44	0.1	130	645982	DIC not installed
TA690-05	144.44	14.44	0.1	130	2090231	DIC not installed
TA690-04	122.22	12.22	0.1	110	2561018	
TA690-03	122.22	12.22	0.1	110	3633850*	failure not in control section
TA690-06	122.22	12.22	0.1	110	5000000	test terminated before failure

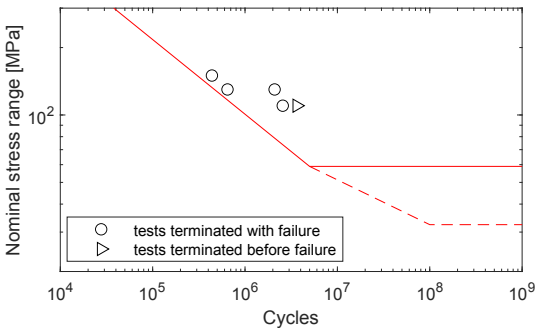

Fig. 5: S-N plot (to be done).

at both locations B and C are presented with the aim of proposing a procedure for sampling a simplified load history, representative of bridge traffic loading, to be applied for variable amplitude fatigue testing.

3.1. CA fatigue test results

The fatigue test data resulting from the experimental investigation are summarized in Table 1, and depicted in Figure 5 together with the characteristic curve corresponding to FAT80 category, i.e. $\Delta\sigma_c = 80$ for $N = 2 \cdot 10^6$ cycles, following the characterization provided in the Eurocode 3 part 1-9, EN 1993-1-9:2006 (2006). This S-N curve corresponds to a 5% probability of failure, and 75% confidence level, intended as a lower bound. Due to the small number of test data, an S-N curve based on the produced data is not derived.

The data are presented considering as load parameter the nominal stress range acting in the control section of the specimen, without considering notch effect. In other words, $\Delta\sigma_{nom} = \Delta F/A_c$, where $A_c = 1000mm^2$ is the cross-section area in the control section and F is the applied force. It can be observed that the fatigue test data are close to the lower bound curve, which is expected due to the fact that the thickness of the attachment plate is greater than the thickness of the loading plate in the control section. This is supported by the circumstance that a larger T_v/T_c ratio increases both the stress concentration factor at the weld toe, and the stress intensity magnification factor for a surface crack growing at the weld toe Radaj et al. (2006). It should be noted that for the current specimen the attachment misalignment is minimized due to the circumstance that the attachment plate is one, and not two as it usually happens in cruciform joints.

Figure 6 shows the macroscopic fracture surface of specimen TA690-04. Multiple crack initiation sites can be observed along both the weld toes. This evidence is given by the presence of multiple ratchet marks, indicating crack coalescence sites. It should be noted that only a few of them have been highlighted in the figure. The leading crack is located approximately in the center of the specimen, and it grew coalescing with smaller cracks. This determines that the shape of the critical crack, i.e. at the onset of failure, is so shallow that it is nearly like an extended surface crack. The presence of numerous crack nucleation sites leads to the consideration that the load level is significantly higher than the fatigue limit, intended as the threshold stress range for small surface cracks.

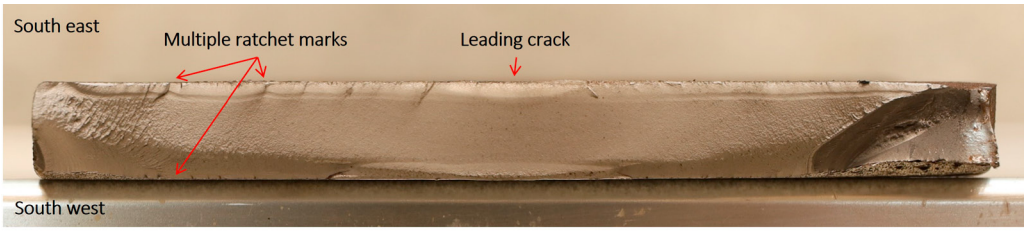

Fig. 6: Macroscopic fracture surface features, specimen TA690-4.

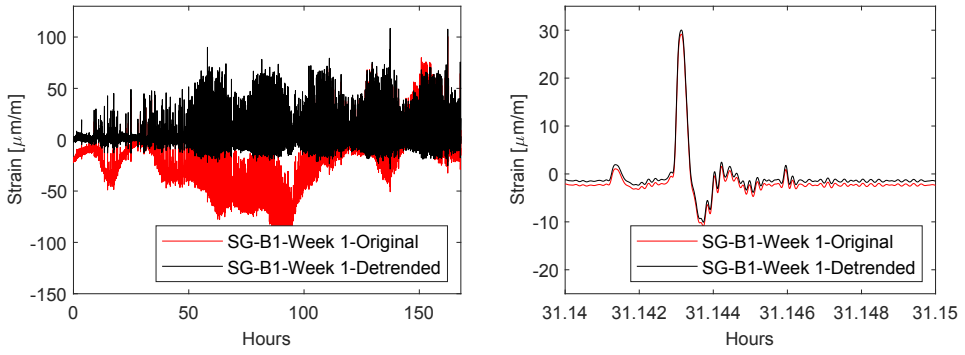

(a) week of measurement (b) effect of passing vehicle

Fig. 7: Strain signal acquired at the bottom flange of the girder in location B.

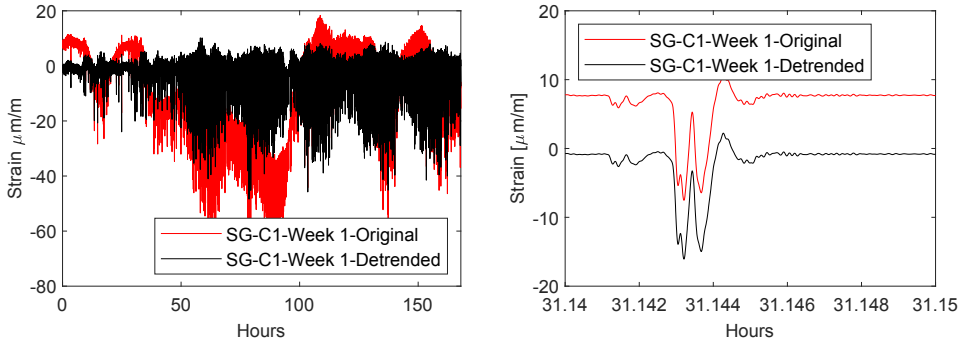

(a) week of measurement (b) effect of passing vehicle

Fig. 8: Strain signal acquired at the bottom flange of the girder in location C.

3.2. Simulated VA traffic load history

Figures 7-8 show a comparison between the strain measurements due to passing vehicles at locations B and C. Due to the different influence lines a the two locations, the strain signals are significantly different, i.e. determining a positive offset for location B and a negative offset for location C. Both the strain gauge signals have been first detrended as described in Section 2.2, and are shown in Figures 7-8 as black lines. By comparing the original and the detrended signals it can be observed that the shape of the signal is preserved, and also the amplitude with respect to the strain value that is read without traffic load.

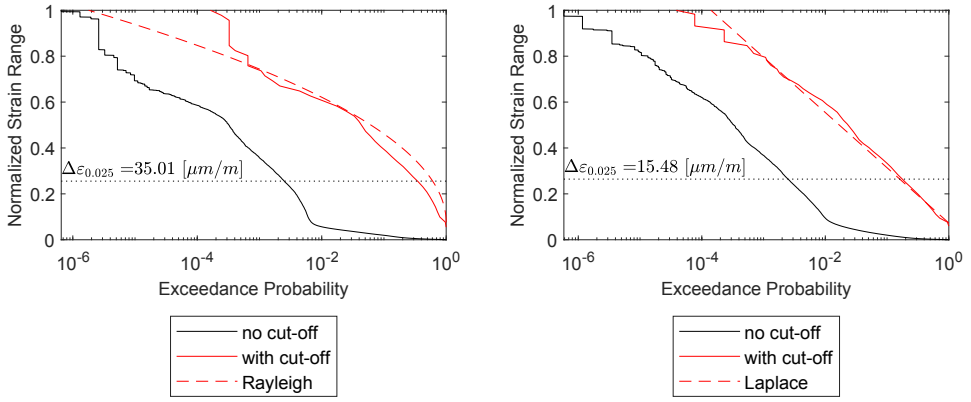

(a) Location B (b) Location C

Fig. 9: Normalized cumulative spectra resulting from the Rainflow counting.

The cumulative spectra resulting from the Rainflow counting are plotted in Figure 9 as black lines. Also, for each of the two strain histories the 0.25% exceedence strain range, $\Delta\varepsilon_{0.25}$, is highlighted in the figure. As is it described in the previous section, this strain range has been used to identify the range filter value, $\Delta\varepsilon_R$ for neglecting small strain ranges, which marginally contribute to the cumulative damage. By neglecting these small strain range values, the cumulative spectra obtained are plotted as a red line. It can be noted that applying the range filter significantly reduces the number of counted load cycles. In fact, $\Delta\varepsilon_R$ roughly corresponds to the knee point observed at an exceedence probability roughly equal to 10^{-2}. In turn, this means that by considering the cut-off, the total number of cycles is less than 1% than those obtained by applying the Rainflow to the original signal. Moreover, the shape of the spectra obtained considering the range filter can be considered to be closer to the shape of the Rayleigh spectrum for location B, and closer to a Laplace spectrum for location C:

$$P\left[\frac{\Delta\varepsilon}{\Delta\varepsilon_{RMS}}\right] = exp\left[-k\left(\frac{\Delta\varepsilon}{\Delta\varepsilon_{RMS}}\right)^{\frac{1}{k}}\right] \tag{2}$$

where $\Delta\varepsilon_{RMS}$ is the root mean square of the process, $P[\Delta\varepsilon/\Delta\varepsilon_{RMS}]$ is the probability of load exceedence, and $k = 0.5$ for the Rayleigh or $k = 1.0$ for the Laplace (linear).

Successively, for each weekly strain history, the signal is condensed into a peak-to-trough history prior to a weekly Markov transition matrix. All weekly Markov transition matrices are then combined by calculating each α_{ij} as the average weighted by the weekly number of cycles. The combined Markov transition matrix is shown for both B and C locations in Figure 10. The distribution resulting from the Markov transition matrices also suggests that, see Gurney (2006): (a) for location B the load history ensembles a narrow-band variable amplitude load history with roughly minimum mean stress and variable peak stress; (b) or location C, the load history ensembles a wide-band variable amplitude load history with variable mean stress and amplitude.

The transition matrices are used to sample the strain history for both locations B and C, making a comparison with the original signal. For each location, a portion of the original and the sampled signals are shown in Figure 11. Moreover, it should be noted that the original signals shown in Figures 11a, 11c have been detrended, as described in Section 2, and furthermore reduced to solely peak-to-troughs transitions, therefore losing the time-scale. It can be observed that the signal generated using the Markov transition matrix preserves the typical trend of the original (reduced) signal. Small differences in the amplitude of the strain fluctuations are due to the randomization of the

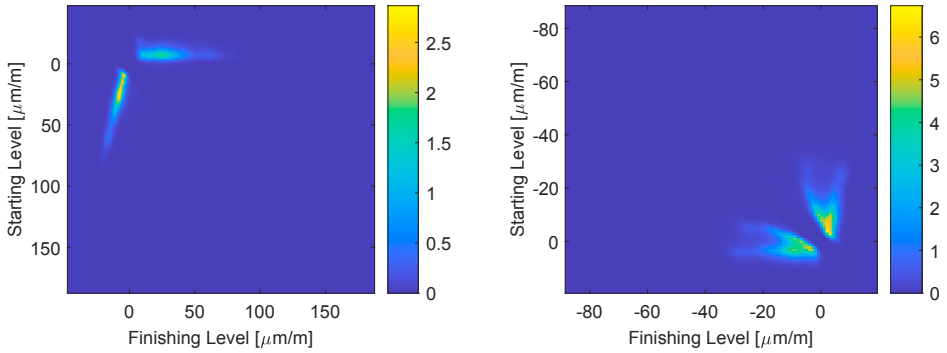

(a) Location B, average of 16097 reversals (b) Location C, average of 28960 reversals

Fig. 10: Visualization of the Markov transition matrices. The scale of the plot is multiplied by 10^{-3}.

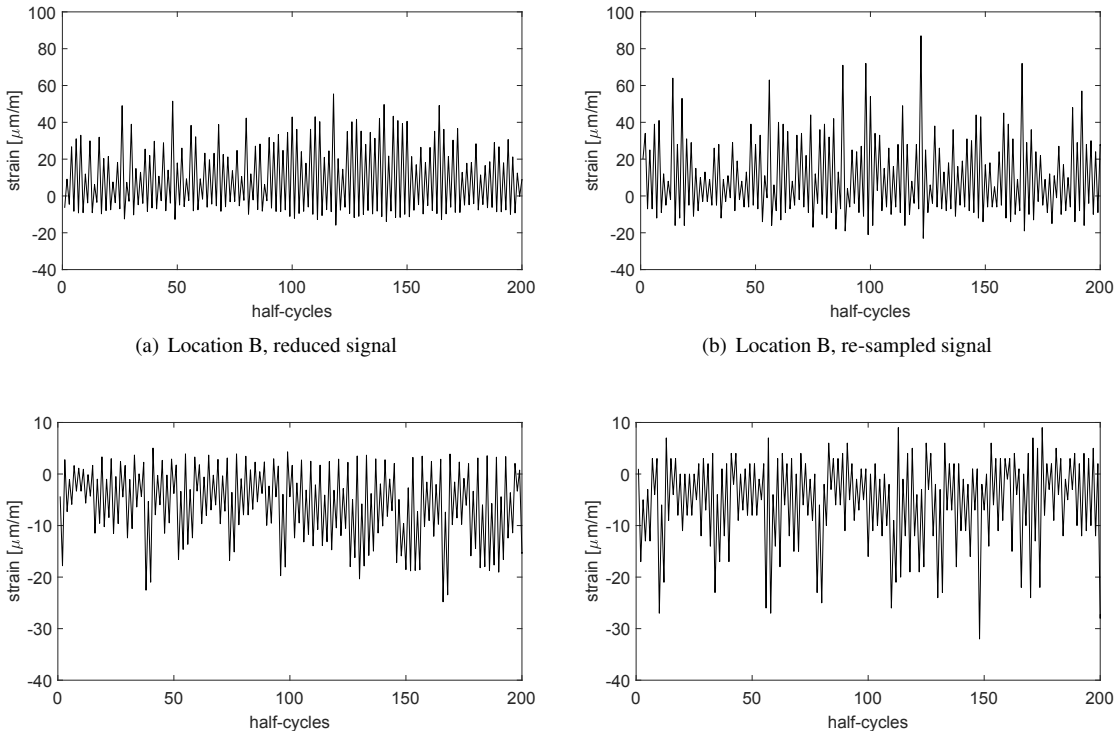

(a) Location B, reduced signal (b) Location B, re-sampled signal

(c) Location C, reduced signal (d) Location C, re-sampled signal

Fig. 11: Visualization of the Markov transition matrices. The scale of the plot is multiplied by 10^{-3}.

procedure. This is more evident in location C, where the passage of single axles is self-evident, and this feature is also reported in the re-sampled signal.

4. Conclusions

The analyses reported in the present paper led to the following conclusions:

- The fatigue resistance of thick transverse attachments, i.e. with the thickness of the attachment plate being double the thickness of the main plate, is close to the lower bound curve FAT80.
- A representative load history can be constructed based on strain measurements conducted on an operating structure. However, verification of different structures is required to make this generalization more robust.
- To reduce the complexity of the acquired strain history, the strain range related to a 0.25% probability of being exceeded is suitable to define strain ranges to be filtered, when the strain history considered is obtained from weekly measurements.
- The strain history due to traffic load can be successfully sampled from the Markov transition matrix constructed by the strain history measured in during operation.

References

Albrecht, P., Lenwari, A., 2009. Variable-amplitude fatigue strength of structural steel bridge details: review and simplified model. Journal of Bridge Engineering 14, 226–237.

Banno, Y., Kinoshita, K., 2022. Experimental investigation of fatigue strength of out-of-plane gusset welded joints under variable amplitude plate bending loading in long life region. Welding in the World , 1–14.

De Jonge, J., 1982. The analysis of load time histories by means of counting methods. NLR MP 82039 U .

EN 1993-1-9:2006, 2006. Eurocode 3: Design of steel structures – Part 1-9: Fatigue. CEN.

Fisher, J.W., 1993. Resistance of welded details under variable amplitude long-life fatigue loading. volume 354. Transportation Research Board.

Fisher, J.W., Mertz, D.R., Zhong, A., 1983. Steel bridge members under variable amplitude long life fatigue loading. Transportation Research Board, National Research Council.

Garcia, M.A.R., 2020. Multiaxial fatigue analysis of high-strength steel welded joints using generalized local approaches. Technical Report. EPFL.

Gurney, T.R., 1979. Fatigue of welded structures. CUP Archive.

Gurney, T.R., 2006. Cumulative damage of welded joints. Woodhead Publishing.

Haibach, E., 1971. The allowable stresses under variable amplitude loading of welded joints, in: Proc. Conf. Fatigue Welded Structures, 1971, The Welding Institute. pp. 328–339.

Heuler, P., Seeger, T., 1986. A criterion for omission of variable amplitude loading histories. International Journal of Fatigue 8, 225–230.

Hobbacher, A., et al., 2016. Recommendations for fatigue design of welded joints and components. volume 47. Springer.

ISO 12110-1:2013, 2013. Metallic Materials—Fatigue Testing—Variable Amplitude Fatigue Testing— Part 1: General Principles, Test Method and Reporting Requirements. ISO.

Klippstein, K., Schilling, C., 1976. Stress spectrums for short-span steel bridges. ASTM International.

Klippstein, K.H., Schilling, C.G., 1989. Pilot study on the constant and variable amplitude behavior of transverse stiffener welds. Journal of Constructional Steel Research 12, 229–252.

Lassen, T., Recho, N., 2013. Fatigue life analyses of welded structures: flaws. John Wiley & Sons.

Matsuishi, M., Endo, T., 1968. Fatigue of metals subjected to varying stress. Japan Society of Mechanical Engineers, Fukuoka, Japan 68, 37–40.

Pereira Baptista, C.A., 2016. Multiaxial and variable amplitude fatigue in steel bridges. Technical Report. EPFL.

Radaj, D., Sonsino, C.M., Fricke, W., 2006. Fatigue assessment of welded joints by local approaches. Woodhead publishing.

Sonsino, C.M., 2004. Principles of variable amplitude fatigue design and testing. Journal of ASTM International 1, 1–21.

Sonsino, C.M., 2007. Fatigue testing under variable amplitude loading. International Journal of Fatigue 29, 1080–1089.

Tilly, G., Nunn, D., 1980. Variable amplitude fatigue in relation to highway bridges. Proceedings of the Institution of Mechanical Engineers 194, 259–267.